Predictive modelling of ASDEX-Upgrade liquid metal divertor experiment

J. Cecrdle[1,2)], J.G.A. Scholte[3)], J. Horacek[1)], T.W. Morgan[3,4)], K. Krieger[5)], A. Manhard[5)], D. Tskhakaya[1)] and the ASDEX Upgrade Team

[1)]Institute of Plasma Physics of the CAS, U Slovanky 2525/1a, 182 00 Prague 8, Czech Republic
[2)]Department of Physics, Faculty of Nuclear Sciences and Physical Engineering, Czech Technical University in Prague, Brehova 78/7, 115 19 Prague, Czech Republic
[3)]Eindhoven University of Technology, Department of Applied Physics and Science Education, De Groene Loper 19,5312 AP Eindhoven, The Netherlands
[4)]Dutch Institute for Fundamental Energy Research, De Zaale 20, 5612 AJ Eindhoven, The Netherlands
[5)]Max Planck Institute für Plasma Physik, Boltzmannstr. 2, 85748 Garching, Germany
Corresponding author email: cecrdle@ipp.cas.cz

Keywords: Divertor, Liquid metal, ASDEX Upgrade, CPS

Abstract

A liquid metal Capillary Porous System (CPS) test module filled with tin was studied in the ASDEX Upgrade (AUG) outer divertor. The CPS module was flush mounted as part of a target tile and exposed using the AUG divertor manipulator. In order to predict tin erosion from the designed module under typical ASDEX Upgrade divertor loading conditions the experiment was interpreted using the HeatLMD code. Preceding test exposures of the CPS in the high heat flux facility GLADIS were performed and interpreted by modelling to quantify the thermo-mechanical properties of the module. The results for the reference ASDEX Upgrade discharge indicated a total of $2x10^{15}$ tin atoms (0.4 μg) would be eroded during the exposure, predominantly through temperature enhanced sputtering. The vapour cooling power was predicted to be negligible (5 kW/m^2 at the end of a 5 s exposure with heat flux from the plasma of 2 MW/m^2). The module was expected to be compatible with plasma operation, with tin erosion too low for any significant effect on the plasma performance. However, interpretative modelling of the experimental discharge with the highest exposure time yielded significantly lower tin erosion than observed. To be attributed to tin radiation the experimentally observed increase in total radiative power (1.5 MW) would require $2x10^{18}$ tin atoms (peak calculated erosion rate) to radiate in the core plasma.

Introduction

One of the most pressing issues in construction of DEMO or a future fusion power plant is the heat load on the first wall and especially the divertor [1]. Plasma facing components based on liquid metal technologies could provide a solution to this problem. Capable of withstanding high heat fluxes (>15 MW/m^2 steady-state [2] and >200 MJ m^{-2}s$^{-1/2}$ pulsed [3]), they could provide a viable replacement of the currently utilised solid tungsten-based components [4]. To successfully implement the technologies into designs of future fusion devices a careful assessment of the performance of liquid metal plasma facing components in tokamak conditions is required. A key component of the viability assessment for future fusion devices is the performance of a liquid metal divertor (LMD) under ELMy H-mode plasmas where significant heat loads, >60 MJm^{-2}s$^{-1/2}$ are expected [5].
For this reason, an experimental campaign was executed at the COMPASS tokamak with two LMD modules filled with Li and SnLi alloy exposed to ELMy H-mode plasmas [6]. Another suitable candidate for a liquid metal (tin), was not tested on COMPASS tokamak, as the performance capability of the device in terms of achievable power load and exposure duration was not optimal for such an experiment [7].

A dedicated experimental campaign was carried out at ASDEX Upgrade tokamak (AUG) [8] with an additively manufactured tungsten CPS filled with tin. The objective was to expose the module to diverted L-mode and ELMy H-mode plasmas ($q_\perp \approx 3\text{-}5\ MW/m^2$, $t = 2\text{-}3.5$ s), representing the first test of a Sn-filled test module at the strike point of a diverted tokamak plasma. This was preceded by a test of the module at the high heat flux facility GLADIS [9] (q = 2-8 MW/m^2, t = 2.5-10 s) to confirm the compatibility of the module with AUG divertor plasma conditions before tokamak exposure.

Sn-filled module

A 40x16x25 mm^3 additively manufactured tungsten capillary porous structure (CPS) was installed flush-mounted in a customized divertor tile on a probe head of the AUG divertor manipulator [10] for exposure at the outer divertor target of AUG. The module consists of two parts. At the top is the actual 1.5 mm thick CPS layer with a porosity $\varepsilon_{CPS} = 0.37$ and pore and grain sizes <30 µm. The volume of the CPS layer would have technically allowed the infiltration of 2 g of tin. However, this was reduced to 1.5 g of tin to prevent potential excessive spill of liquid tin under high heat load. The bottom 23.5 mm part was made from solid (but also additively manufactured) tungsten with a porosity of $\varepsilon_{bulk} = 0.12$. Because of the manufacturing process the corresponding material parameters (heat capacity and conductivity) were expected to deviate from those of conventional tungsten [11], and a dedicated measurement was required to obtain them together with those for the CPS layer.

GLADIS experiment

Before being exposed to AUG plasma discharges the module was tested at the high heat flux facility GLADIS [9]. This was required to confirm the compatibility of the module with AUG divertor plasma conditions, both in tin-wetted and unwetted condition, as well as for quantifying the material parameters of the module. The wetted module was exposed to a total of 19 discharges with varying heat fluxes and times (q = 2-8 MW/m^2, t = 2.5-10 s). Discharge #264327 (q = 4 MW/m^2 and t = 3.5 s) was chosen for the benchmark modelling because of optimal heat deposition and diagnostics data (IR camera and pyrometer).

According to [12] the heat conductivity of a porous material can be calculated as $\kappa_{por} = \kappa\frac{1-\varepsilon}{1+11\varepsilon^2}$, where κ is the conductivity of the pure material and ε is the porosity. For tungsten with $\varepsilon_{bulk} = 0.12$ and $\kappa_W = 130$ W/m/K [13], the conductivity of the bulk should be $\kappa_{bulk} = 99$ W/m/K.

For porous materials wetted with a fluid heat conductivity can be calculated as $\kappa_{fill} = \frac{1-\left(1-\frac{b\kappa_f}{\kappa_s}\right)\varepsilon}{1+(b-1)\varepsilon}$, where κ_f is the conductivity of the fluid and κ_s is the conductivity of the solid and $b = \frac{3\kappa_s}{(2\kappa_s+\kappa_f)}$ [14].

For a tungsten CPS with porosity $\varepsilon_{CPS} = 0.37$ and conductivity of tin $\kappa_{Sn} = 26$ W/m/K [13] the resulting conductivity of the CPS layer should be $\kappa_{CPS} = 84$ W/m/K. Volumetric heat capacities of the CPS C_{vCPS} =2.2 MJ/m^3/K and bulk C_{vbulk} = 2.3 MJ/m^3/K were calculated using the rule of mixture, i.e. $C_v = (1-\varepsilon)C_{vW} + (0.8\ \varepsilon C_{vSn})$ with C_{vW} = 2.57 MJ/m^3/K and C_{vSn} = 1.65 MJ/m^3/K [13].

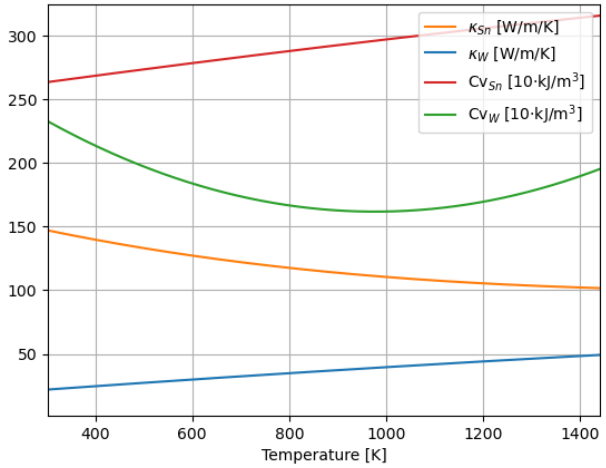

Fig. 2: Temperature dependency of W and Sn heat capacity and conductivity.

The factor 0.8 is attributed to the underfilling of the CPS. All the heat conductivities and capacities were calculated accordingly to the temperature dependence (See Fig. 2)

GLADIS Modelling in HeatLMD

HeatLMD code, described in detail in [7], is a 3D plus temporal code for liquid metal surface and plasma interaction. It consists of a finite element solution of the heat equation, surface erosion (physical and thermal sputtering and evaporation) and subsequent vapour cooling effect. The inputs into the code are relevant plasma parameters at the target surface (electron temperature and density, impacting ion flux and energy, perpendicular heat flux, magnetic field intensity) and the main outputs are the erosion rate, vapour cooling power and the surface temperature.

2D modelling of the module surface temperature evolution during the GLADIS discharge #264327 ($q = 4$ MW/m^2 and $t = 3.5$ s) was done in the HeatLMD code, to validate the estimated heat conductivities and heat capacities of the CPS and the bulk of the module.

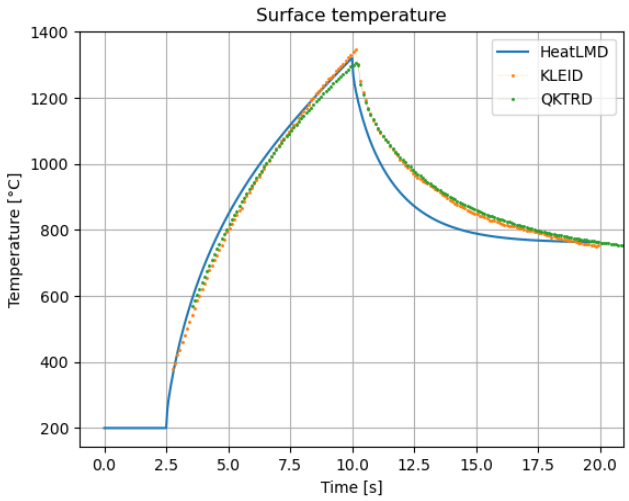

Fig. 3: LMD module surface temperature from HeatLMD, IR camera and pyrometer during GLADIS testing discharge. The discharge starts at 2.5 s.

As seen in Fig. 3 the computed surface temperature closely matched the experimental data during the heating phase $t = 2.5$-10 s, whereas during the cooling phase ($t > 10$ s) there are significant deviations with yet unknown origin. A possible cause of the deviation might be an incorrect thermal conduction in the bulk material. Therefore, a more in-depth analysis is required. The closely matching temperatures at $t = 20$ s (simulated module in thermal equilibrium) suggest the estimation of the volumetric heat capacity (total thermal energy in the module) was correct. The surface temperature of the module decreased further after $t = 20$ s because of the thermal contact with the support structure, which the model did not consider.

No substantial change in the surface temperature evolution over time during simulation runs with different heat conductivities (in range of 42-100 MW/m/K) of the CPS layer was observed. The insensitivity of the model with respect to this parameter implies that the estimation by the modelling has a significant error (+/-50 %). The likely reason was the presence of a drilled hole for installation of an electrical heater element. Because the hole was empty during the GLADIS experiment, it served as a thermal break, decreasing the effective heat transport between the centre of the surface and the bulk material (See Fig. 4). The top part of the module therefore had almost constant temperature from the surface to the depth of the hole over the main part of the discharge, thus strongly reducing the effect of the heat conductivity near the surface. The peak temperature difference between cases with $\kappa = 98$ W/m/K, the conductivity of the bulk, and $\kappa = 42$ W/m/K, half of the expected value, was 75 °C (6% difference). The expected value of $\kappa = 84$ W/m/K was therefore chosen for all following calculations.

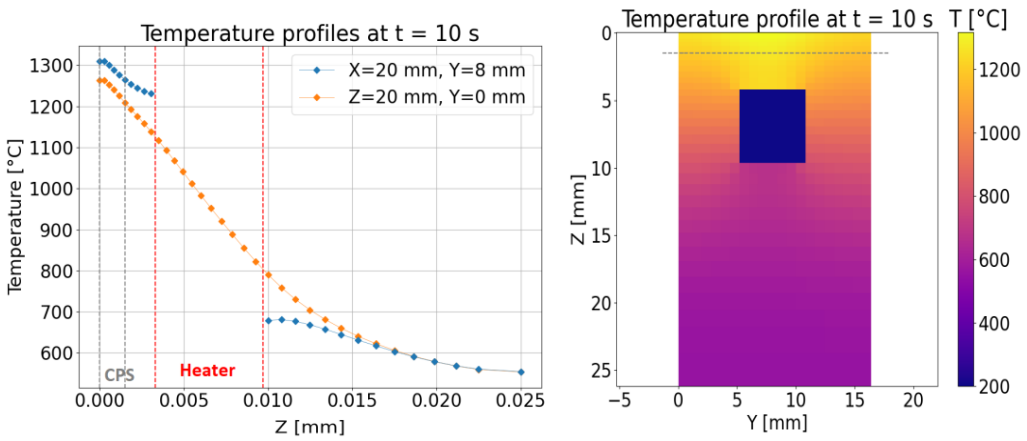

Fig. 4: Calculated temperature profiles of the GLADIS discharge at t = 10 s in the middle (Y = 8 mm) and at the edge (Y = 0 mm) of the target (left) and a 2D profile (right), indicating the conduction suppression effect of the heater hole.

The current structure of HeatLMD code does not allow for a circular heater hole to be implemented, however the square profiled geometry, used in the simulations, was validated by cross-checking with ANSYS modelling with correct geometry (circular hole).

ASDEX Upgrade LMD experiment setup

During the discharges the outer strike-point was initially positioned above the target and then moved down on the CPS surface area for a set time interval and then raised up again to its initial position for plasma ramp down. The exposure interval was increased in subsequent discharges from 0.5 s up to 3.5 s. The time intervals where the CPS was kept in the private flux region of the divertor with insignificant power flux levels were used to obtain in-situ reference data for the effect of the additional Sn source on plasma performance as well as reference data for surface temperature measurements by IR thermography. Moreover, camera inspection of the probe head surface in between discharges was used to obtain visual cues for Sn erosion effects on the plasma performance. The internal temperature of the CPS was monitored by two thermo-couples inserted in holes of different depth (3 mm and 8 mm below the surface).

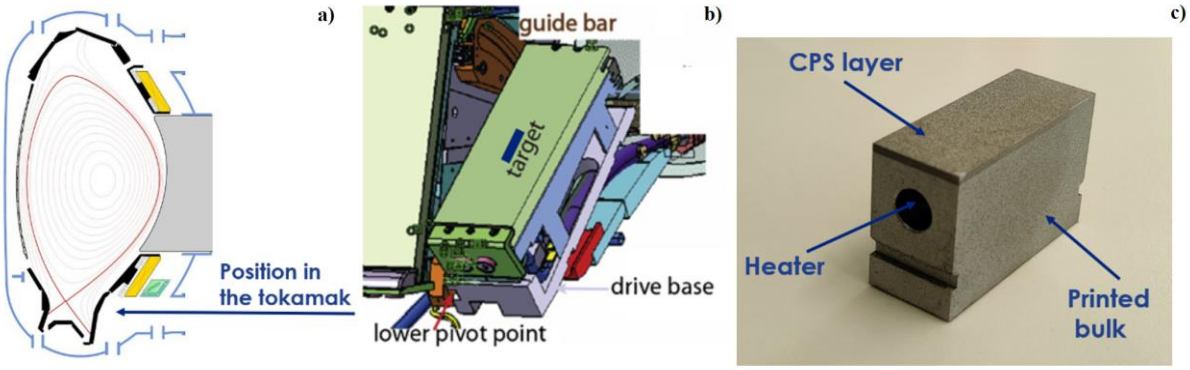

Fig. 1: Schema of the experimental setup : a) Position of the module in the tokamak. b) Outer divertor port manipulator with the position of the module highlighted, edited from [10]. c) Photograph and description of the module.

ASDEX Upgrade modelling in HeatLMD

In order to find the optimal operation scenario for the experiment, a reliable prediction of tin erosion is highly beneficial. The desired scenario for this experiment should provide sufficient tin erosion to cause changes in plasma parameters, most notably total radiation, but not enough to cause radical

changes and potentially plasma disruption. Another key aspect is the tin budget. Since there is no reservoir to replenish the eroded tin in the CPS, the experiment would have to be terminated prematurely if all the tin was lost from the CPS. Apart from a sudden drop in the tin source, there was no means of detecting the total loss of tin from the module, further increasing the importance of the reliable erosion prediction.

Two scenarios for predictive runs and an actual discharge from the experiment were selected for modelling (all ELMy H-mode). The objective of the predictive modelling was to predict expected and worst-case scenarios. The modelling of the actual discharge was done to interpret the observations from the experiment. The HeatLMD code, described in [7], with the addition of a runtime calculation of tin prompt redeposition was used for the erosion modelling. The heating element part, empty hole in the GLADIS case, made from a nichrome wire had a time independent heat conductivity of 11.3 W/m/K and volumetric heat capacity 3.17 MJ/m3/K [15]. The prompt redeposition fraction was calculated via a simple Monte Carlo approach. Every timestep a set of 10^4 escaping tin atoms with normally distributed kinetic energy is generated in each element, enough to provide statistically precise results while not being computationally demanding. Each atom has an ionization mean free path, based on the measured plasma parameters (T_e, n_e) and the normal to surface velocity $v_\perp$ given by the energy of the atom (based in the surface temperature) and scattering angle (cosine distribution). The mean free path is $l_i = v_\perp {T_e}^{3/2}/n_e$. If the atom is ionized within the magnetic presheath, it promptly redeposits. The border of the redeposition area was set as five times the Larmor radius of deuterium ions i.e., $l_i < \frac{5\sqrt{5/2 T_e m_D k_B}}{B_t}$ yields prompt redeposition. The prompt redeposition fraction is then given as the fraction of promptly redeposited atoms from the randomly generated set. This approach is consistent with the comprehensive kinetic modelling of tungsten redeposition in [16]. Similarly to tungsten, tin can be subjected to multiple ionizations within the sheath region, therefore the sheath electric potential is the dominant contributor to prompt redeposition.

Firstly, the reference discharge scenario was simulated for validation. Furthermore, a hypothetical discharge with the highest heating power available was used to simulate the worst-case scenario with 5 s of LMD exposure. Finally, the discharge from the actual experiment with the longest exposure time of the module (3.5 s) was analysed. For each case two simulations with different initial temperatures of T_0 = 230 °C and T_0 = 400 °C respectively were run. For the hypothetical worst-case scenario only the T_0 = 400 °C case was considered. For the experimental discharges the initial temperature was adjusted to T_0 = 230 °C by the CPS heating element. The plasma parameters of the modelled scenarios are listed in Tab. 1.

			Inter-ELM			ELM		
Disch. num.	Type	Exposure time [s]	T_e [eV]	n_e [10^{19}m^{-3}]	$q_\perp$ [MW/m^2]	T_e [eV]	n_e [10^{19}m^{-3}]	$q_\perp$ [MW/m^2]
38988	Reference	5	10	1	2	300	20	20
38320	Hypothetical	5	13	5	6	420	30	50
41279	Experimental	3.5	10	1.5	5	100	60	15

Tab. 1: Typical target plasma parameters at strike point of the modelled discharges.

The perpendicular heat flux was taken from the IR camera measurements. The resolution of the camera is 0.66 ms in time and 0.58 mm per pixel [17]. Electron temperature and density were taken from the AUG triple probe array. The temporal resolution of the probes is 45 µs and the spatial resolution is 2.5 cm (at the location of the module). Because of the bias voltage of the probes being too low, the probes cannot measure valid electron temperatures during ELMs. The target electron temperature during ELMs was taken as 0.7 of the pedestal electron temperature obtained from the integrated data analysis (IDA) [18], consistently with results on JET [19].

Discharge number	Initial temperature [°C]	Maximal surface temperature [°C]	Eroded atoms [10^{17}]	Eroded mass [µg]
38988	230	620	2	40
38988	400	790	3	60
38320	400	1120	250	5000
41279	230	980	20	400

Tab. 2: Resulting maximal surface temperature and erosion of the modelled discharges.

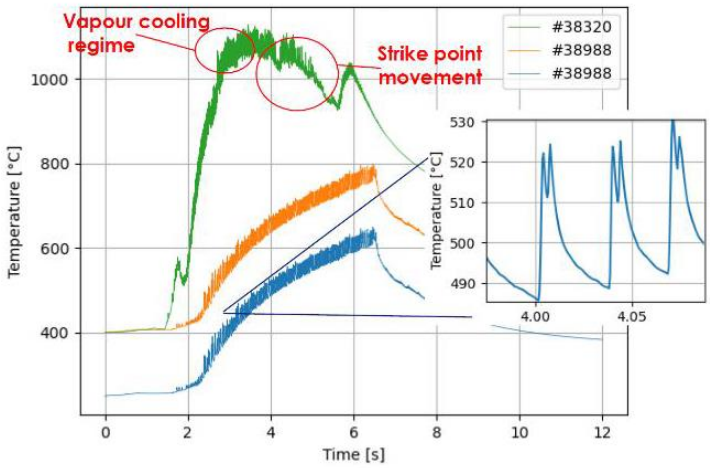

Fig. 5: Maximal surface temperature evolution for the predictive modelling scenarios.

The resulting maximal surface temperatures and erosions are listed in Tab. 2. The temperature evolution of the modelled scenarios is shown in Fig. 5. The predicted peak surface temperature for the reference discharge of 620 °C is well below the limit for significant tin erosion (evaporation) >1000 °C [19], resulting in a total of $2x10^{17}$ of eroded atoms escaping into the divertor plasma. As expected, the maximal surface temperature of the 400 °C scenario is 170 °C higher (the temperature curve is essentially shifted upwards) resulting in a 50% increase of total tin erosion. Even the higher value of $3x10^{17}$ tin atoms is still not expected to have a significant effect on the plasma discharge. In both of these scenarios the dominant erosion effect is the thermally enhanced sputtering.

In contrast, for the hypothetical worst-case scenario the code predicts release of $2.5x10^{19}$ (5 mg) tin atoms into the divertor plasma, sufficient to affect the discharge by corresponding radiation losses. Even though the peak surface temperature is only 1120 °C, temperature saturation by vapour cooling is observed for approximately 1 second, before the strike-point moves. This effect is normally observed at temperatures >1600 °C [20,21]. A possible explanation of this is the very high plasma density at the target causing higher than typical cooling energy per particle, thus yielding higher vapour cooling power at lower surface temperatures. This is in line with the results in [22] where temperature saturation of a Li LMD occurred at 500 °C due to high plasma density, whereas normally it occurs at T >900 °C [7,20]. This phenomenon however requires further investigation and ideally experimental verification as it has been seen only in simulations so far.

Experiment modelling and data analysis

Since the IR camera observing the module had a very poor spatial resolution, only a few pixels were observing the module surface. Therefore, comparison of surface temperature evolution between the simulation and experimental data was not trivial. Although the data do show a correlation (See Fig. 6), the deviation is notable. Especially between t = 4-6 s, where the rate of temperature increase temporarily decreases. This occurs during the time where the strike point was at a constant location, therefore an unaccounted physical effect, such as a change in emissivity or the structure of the liquid tin and CPS surface, likely distorted the IR camera data. This could have been the case in the post exposure cooling phase as well. The sudden drops in measured temperature at t = 7 s and t = 8.5 s indicate that another reason for the deviation might be a shift of the camera line of sight. Since the module was observed by a wide-angle camera and only a few pixels positioned on the module.

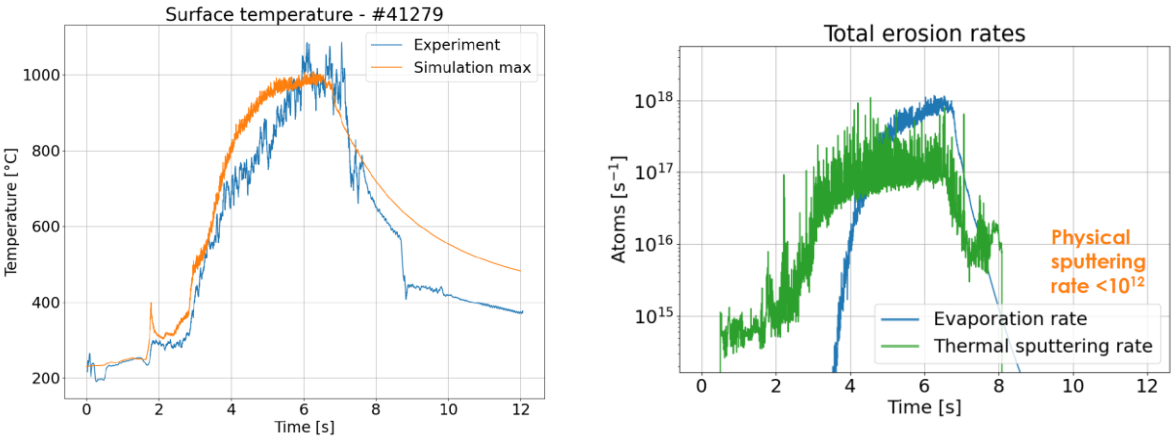

Fig. 6: Calculated and measured surface temperature (left) and calculated erosion rate from sputtering and evaporation (right) of the modelled experimental discharge.

Unlike for the reference discharge, the measured and predicted surface temperature during the experimental discharge did reach a sufficiently high value for evaporation becoming the dominant erosion effect (around 800 °C). Nevertheless, the surface temperature and plasma parameters were not sufficient to reach the vapour cooling regime, the saturation of the surface temperature at t = 6 s was most likely caused by a decrease of heat flux (measured by IR camera at a location 180° toroidally from the module), likely caused by an increase in radiation from the plasma.
Individual ELM heat shocks increased the surface temperature by ≈ 50 °C, comparable to the increase observed during the COMPASS experiment [7]. The increase in erosion depended on the phase of the discharge. Initially the increase was by an order of magnitude, in the sputtering-dominated phase, and later after surface temperature increase over 800 °C in the evaporation-dominated phase the erosion rate was approximately doubled during ELMs.

During the experimental discharges with long LMD strike point exposure a gradual increase in total radiation was observed, as can be seen in Fig. 7. In case of the modelled discharge, the increase was by 50% at the peak compared to discharges where the module was not exposed to the strike point.

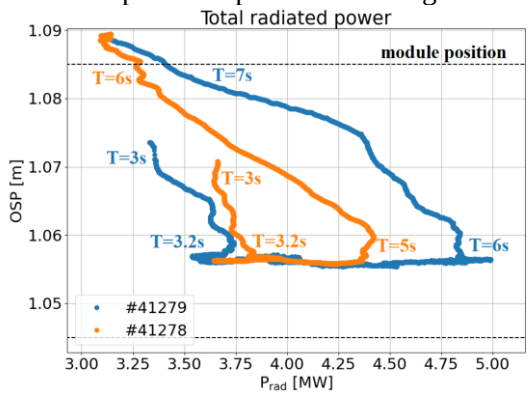

Fig. 7: Corelation of the increase in total radiation and the position of the strike point.

The correlation of the radiation increase with the position of the strike point is apparent in Fig. 6. The outer strike point (OSP) is located above the module at the beginning of the discharge and is subsequently shifted to approximately the middle of the module surface. In the period of constant OSP position, the total radiation gradually increases, corresponding to the steepest part of the surface temperature increase. After the strike point is moved back to its position above the module, the total radiation from the plasma begins to drop. This indicates, together with the fact that the increase was not observed during discharges with no exposure, that the excess radiation indeed originates from the tin contamination of the plasma.
The peak excessive radiation during discharge #41279, was P_{ex} =1.5 MW (50% increase).
The modelled peak erosion rate was 2×10^{18} atoms per second. This number of tin atoms could radiate 1.5 MW if present in the core plasma, radiating 40 MeV/particle/s at Te = 1 keV and ne = 5×10^{19} m^{-3} [22]. However, it would require a very high percentage of the atoms actually reaching the core plasma region, which is unlikely because of divertor impurity retention [23].

If the increase in total radiation cannot be explained by the erosion from sputtering and evaporation alone, another source of tin must have been present. For that there are two possible mechanisms currently deemed plausible. The first one is a tin leak located on the neighbouring manipulator tile (see Fig. 8), which already appeared during one of the first discharges and not during the modelled one. The second is ejection of a large number of tiny tin droplets from capillary unbound tin pools on the surface of the module [25]. Ejection of just a few large droplets can be ruled out because it would lead to radiation spikes rather than the observed gradual increase. Which of these two mechanisms is responsible for the large increase remains to be validated.

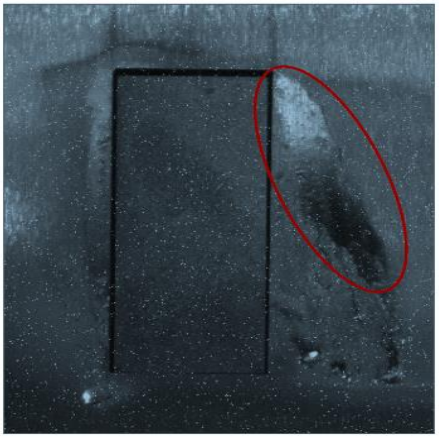

Fig. 8: Post discharge photograph of the module with a visible tin splash

Conclusion

A dedicated experiment with with an LMD-mock-up consisting of an additively manufactured W CPS infiltrated with was conducted at ASDEX Upgrade. The module was exposed to both L-mode and ELMy H-mode plasmas. Preceding test exposures of the LMD module in the high heat flux facility GLADIS experiment were modelled with the HeatLMD code to determine the thermo-mechanical material parameters of the module. The resulting parameters for the CPS layer are κ_{CPS} = 84 W/m/K, 2.2 MJ/m^3/K and for the module bulk material κ_{bulk} = 99 W/m/K and C_{vbulk} =2.3 MJ/m^3/K. In order to predict tin erosion in plasma exposures, the HeatLMD code was used to simulate a reference discharge and a hypothetical worst-case scenario with maximal power available with predicted total erosion of 2-3x10^{17} and 2.5x10^{19} tin atoms respectively. For interpretation of experimental data, also the discharge with the longest module exposure interval was simulated. The derived total number of tin atoms lost to the divertor plasma was 2x10^{18} atoms, dominantly by evaporation. During the discharge with the longest exposure interval a significant increase in total radiation was observed, not readily explainable by only tin sputtering and evaporation. Possible additional tin sources responsible for the excess tin in the plasma might be either a large splash of ejected tin deposited at the adjacent tile surface in one of the first discharges, or small droplet ejection, or both. Further analysis of the underlying processes is required to resolve the discrepancy.

Acknowledgements

This work was conducted with the support of the Czech Science Foundation project GACR 22-03950S.

This work has been carried out within the framework of the EUROfusion Consortium, funded by the European Union via the Euratom Research and Training Programme (Grant Agreement No 101052200 —EUROfusion). Views and opinions expressed are however those of the author(s) only and do not necessarily reflect those of the European Union or the European Commission. Neither the European Union nor the European Commission can be held responsible for them.

References

[1] J. H. You, *et al.*, 2022, Fus. Eng. Des. **175** 113010
[2] T. W. Morgan. *et al.*, 2017, Nucl. Mat. Energy **12** 210-215
[3] A. V. Vertkov and V. A. Evtikhin, 2009, Plasma Dev. Op. **4** 265-285
[4] F. L. Tabares, *et al.*, 2017, Nucl. Fusion **57** 016029 (11pp)
[5] T, Eich, *et al.*, 2017, Nucl. Mat. Energy **12** 84-90
[6] R. Dejarnac, *et. al.*, 2020, Nucl. Mat. Energy **25** 100801
[7] J. Horacek, *et al.*,2020, Nucl. Mat. Energy **25** 100860
[8] H. Meyer, *et al.*, 2020 Nucl. Fusion **59** 112014
[9] H. Greuner, *et al.*, 2007 J. Nuc. Mat. 367-370 1444-1448
[10] A. Herrmann, *et al.*, 2015, Fus. Eng. Design **98-99** 1496-1499
[11] A. E. Gheribi, *et al.*, 2015, Appl. Phys. Lett. **107** 094102
[12] J. C. Y. Koh and A. Fortini, 1973 Int. J. Heat Mass Transf. **16** 2013-1022

[13] W. Woodside, 1958, Can. J. Phys. **36** 815
[14] R. W. Powell, C. Y. Ho and P. E. Liley, 1966, Nat. Bur. Stand. Thermal Conductivity of Selected Materials
[15] P. Majumder and A Bhattacharyya,2008, Modelling Simul. Mater. Sci. Eng. **16** 015006
[16] D. Tskhakaya,*et al.*, 2015, J. Nuc. Mat. **463** 624-628
[17] B. Sieglin, *et al.*, 2015, Rev. Sc. Inst. **86** 113502
[18] R. Fischer, *et. al.*, 2017, Fus. Sc. Tech. **58** 675-684
[19] J. Adamek, *et al.*, 2020, Nucl. Fusion **60** 096014
[20] T. W. Morgan, *et al.*, 2018, Plasma Phys. Control. Fusion **60** 014025
[21] G. Mazzitelli, *et al.*, 2019, Nucl. Fusion **59** 096004
[22] J. Cecrdle, 2021 Msc. Thesis, FNSPE CTU
[23] H. K. Chung, *et al.*, 2005, High En. Dens. Phys. **1** 3-12
[24] A. Geier, *et al.*, 2002, Plasma Phys. Control. Fusion **44** 2091-2100
[25] W. Ou, *et al.*, 2021, Nucl. Fusion **61** 066030